Astronomy & Astrophysics manuscript no. poker
April 18, 2011

POKER: Estimating the Power Spectrum of diffuse Emission with complex Masks and at high angular Resolution

N. Ponthieu, J. Grain, G. Lagache

IAS, Institut d'Astrophysique Spatiale, CNRS Université Paris 11, Bâtiment 121, 91405 Orsay, France

April 18, 2011

Abstract

We describe the implementation of an angular power spectrum estimator in the flat sky approximation. POKER (P. Of k EstimatoR) is based on the MASTER algorithm (Hivon et al 2002) developed in the context of CMB anisotropy. It works entirely in discrete space and can be applied to arbitrary high angular resolution maps. It is therefore particularly suitable for current and future infrared to sub-mm observations of diffuse emission, whether Galactic or Cosmological. The code is publicly available at `http://www.ias.u-psud.fr/poker`.

Key words. Cosmology – Diffuse emission – Infrared – sub millimeter – CIB – power spectrum – statistics

1. Introduction

Whether it is due to Galactic dust or synchrotron, to cosmological backgrounds such as the Cosmic Microwave Background (CMB) or the Cosmic Infrared Background (CIB) that traces the integrated radiation of unresolved galaxies, diffuse emissions are omnipresent in infrared and millimetric observations. The angular power spectrum of such radiations is one of the main tools to constrain the structure of the Interstellar Medium, the clustering of IR galaxies (CIB) or the cosmological parameters (CMB). In short, its estimation requires to Fourier transform the image and to average its modulus square into frequency bins. However, the image has boundaries and often masked regions (e.g. to remove bright point sources) which induce power aliasing and biases the estimation of the power spectrum if not accounted for properly. The effect becomes quite significant when the signal has a steep power spectrum like k^{-3} as measured for Galactic cirrus emission (Miville-Deschênes et al 2007) or even steeper than k^{-4} as for CMB anisotropy at angular scales smaller than a few arcmin (see e.g. Reichardt et al 2009, Brown et al 2009). Recently, to account for non periodic boundaries Das et al 2009 have proposed an original apodizing technique that helps to deconvolve the estimated power spectrum from that of the observed patch boundaries. They also mitigate the impact of holes by a pre-whitening technique applied to data in real space.

In the context of CMB anisotropy, Hivon et al 2002 have developed the MASTER method that allows to correct for mask effects on the output binned power spectrum. They work on the full sky and account for its curvature. Instead of classical Fourier analysis, they project the data onto spherical harmonics and go through the algebra of *pseudo* angular power spectra (see Sect. 2). This idea has been successfully used in several experiments (e.g. de Bernardis et al 2000, Benoît et al 2003) and is also the basis of more refined algorithms used in e.g. WMAP (Hinshaw et al 2003) and Archeops (Tristram et al 2005). However, direct use of MASTER in the context of infrared observations with a resolution of typically a few arcsec requires to estimate Legendre polynomials up to orders ℓ of 10,000 or more for which current recurrences and integration methods are numerically unstable. Other techniques developed in the context of CMB anisotropy such as maximum likelihood estimation (Bond et al 1998) could be transposed to high resolution maps, but the numerical cost $\propto n_{pix}^3$ is prohibitive for common applications when the analysis pipeline requires Monte-Carlo simulations.

This paper aims at transposing the *pseudo*-spectrum approach pioneered by MASTER to the context of high resolution observations and classical Fourier analysis in the flat sky approximation. Its originality compared to other approaches is that it works exclusively in discrete space and therefore avoids the complexity of resampling the data and integrating Bessel functions. Our algorithm was nicknamed POKER, for "P. Of k EstimatoR". The paper is organized as follows. Section 2 provides the definitions and algebra involved in POKER and Sect. 3 shows its applications on simulations of various astrophysical components spectra and a non trivial mask. Detailed derivations of our results are postponed to appendices.

2. Power spectrum estimation on an incomplete observation of the sky

We first briefly state the limits of the flat sky approximation, then we recall the definitions of the power spectrum and *pseudo*-power spectrum of data in the context of continuous Fourier transforms. Finally, we move to its counterpart in discrete space and to the implementation of POKER.

Send offprint requests to: N. Ponthieu, e-mail: `Nicolas.Ponthieu@ias.u-psud.fr`

2.1. Flat sky approximation

Projecting an observed fraction of the sky on the tangential plane alters the image properties in a way that depends on the specific reprojection scheme (e.g. gnomonic, cylindrical etc.). To first order, two points at a distance $d\theta$ on the sphere appear at a distance $\tan(d\theta)$ on the plane. The difference between the two is typically 1% for $d\theta = 10°$. It therefore makes sense for observations whose sky fraction are a few degree wide to neglect the curvature effect and assume the sky is flat (see e.g. Pryke et al 2009).

2.2. Continuous Fourier Analysis and masked Data

On such a flat 2-dimensional surface, a scalar field $T_{\boldsymbol{r}}$ depending on the direction of observation $\boldsymbol{r}$ is represented in Fourier space by

$$T_{\boldsymbol{k}} = \int_{-\infty}^{\infty} d\boldsymbol{r} T_{\boldsymbol{r}} e^{-i\boldsymbol{k}\cdot\boldsymbol{r}}, \tag{1}$$

$$T_{\boldsymbol{r}} = \int_{-\infty}^{\infty} \frac{d\boldsymbol{k}}{(2\pi)^2} T_{\boldsymbol{k}} e^{i\boldsymbol{k}\cdot\boldsymbol{r}}. \tag{2}$$

For a random isotropic process, the 2D-power spectrum $\mathcal{P}_{\boldsymbol{k}}$ is defined as

$$\langle T_{\boldsymbol{k}} T^*_{\boldsymbol{k}'} \rangle \equiv \mathcal{P}_{\boldsymbol{k}} \delta_{\boldsymbol{k}-\boldsymbol{k}'} \tag{3}$$

where brackets denote statistical average. We denote by 1D-power spectrum its azimuthal average:

$$P_k \equiv \frac{1}{2\pi} \int_0^{2\pi} d\theta \; T_{\boldsymbol{k}} T^*_{\boldsymbol{k}} \; . \tag{4}$$

P_k is the physical quantity of interest which we want to reconstruct. It is the Fourier transform of the 2-point correlation function. If the process is isotropic, the 2D and 1D-power spectra are related by

$$\langle T_{\boldsymbol{k}} T^*_{\boldsymbol{k}'} \rangle \equiv \mathcal{P}_{\boldsymbol{k}} \delta_{\boldsymbol{k}-\boldsymbol{k}'} = (2\pi)^2 P_k \delta_{\boldsymbol{k}-\boldsymbol{k}'}, \tag{5}$$

In the following, we will drop the 1D or 2D qualifiers for readability and use indifferently the term power spectrum, unless the difference needs to be emphasized. In practice however the integrals of Eqs. (1, 2) cannot run up to infinity simply because of the limited size of the observation patch. This is accounted for by a weight function $W_{\boldsymbol{r}}$ applied to the data. Its most simple form is unitary on the data, zero outside the observation range or where strong sources are masked out. More subtle choices such as inverse noise variance weighting or apodization (cf. Sect. 3) are usually used. Instead of the true Fourier amplitudes, we are then bound to measure the amplitudes of the masked data, a.k.a. the *pseudo*-amplitudes

$$\hat{T}_{\boldsymbol{k}} = \int_0^{\infty} d\boldsymbol{r} T_{\boldsymbol{r}} W_{\boldsymbol{r}} e^{-i\boldsymbol{k}\cdot\boldsymbol{r}}. \tag{6}$$

Equation (4) applied to the *pseudo*-amplitudes gives the 1D-*pseudo*-power spectrum

$$\hat{P}_k = \int_0^{\infty} k_1 dk_1 \; K_{kk_1} P_{k_1}, \tag{7}$$

where K_{kk_1} is the mixing matrix that depends on the weighting function $W_{\boldsymbol{r}}$, the beam and filtering transfer functions. Determining the signal power spectrum requires to solve this equation for P_{k_1}. A detailed derivation of the analytic solution can be found in Hivon et al 2002.

2.3. Discrete Fourier Analysis and POKER

Any data set is by construction discretely sampled. Computing the quantities defined in the previous section requires mathematical interpolation and/or resampling of these data and appropriate integration tools, especially if the underlying data power spectrum is steep as for galactic cirrus whose $P(k) \sim k^{-3}$ (Miville-Deschênes et al 2007). Rather than dealing with these difficulties, we keep the native pixelized description of the data and work completely in discrete space. We use the Discrete Fourier Transform (hereafter DFT) as provided by data analysis softwares. For a map of scalar quantity $D_{\mu\nu}$ and of size $N_x \times N_y$ pixels, it is defined as

$$D_{mn} = \frac{1}{N_x N_y} \sum_{\mu,\nu} D_{\mu\nu} e^{-2i\pi(\mu m/N_x + \nu n/N_y)}, \tag{8}$$

$$D_{\mu\nu} = \sum_{m,n} D_{mn} e^{+2i\pi(\mu m/N_x + \nu n/N_y)}. \tag{9}$$

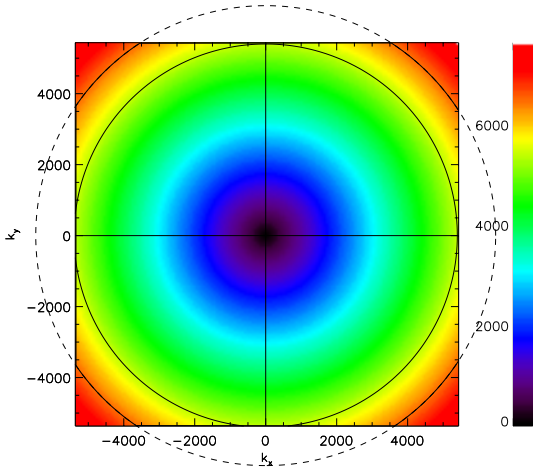

Figure 1. Map of the Fourier modes of the worked examples of Sect 3. The inner circle delimits the Nyquist range. Modes that lie on the outer circle are examples of modes of larger modulus then $k_{Nyquist}$. For such modes, not all directions are sampled in the Fourier plane (dashes represent the missing modes).

Throughout this work, although we will denote quantities in direct and Fourier space by the same name, Greek indices will denote pixel indices in real space whereas roman indices will refer to amplitudes in Fourier space. Unless stated otherwise, sums over μ and m (resp. ν and n) run from 0 to $N_x - 1$ (resp. $N_y - 1$). $\Delta\theta$ is the angular resolution of the map in radians. For a given wave-vector $\boldsymbol{k}_{mn}$, labelled by the m and n indices, its corresponding norm is denoted by $k_{mn} = (2\pi/\Delta\theta)\sqrt{(m'/N_x)^2 + (n'/N_y)^2}$ with $m' = m$ (resp. n') if $m \leq N_x/2$ and $m' = N_x - m$ if $m > N_x/2$. This convention ensures that on small angular scales k matches the multipole ℓ used in the description of CMB anisotropy. The Nyquist mode is $\pi/\Delta\theta$.

It is well known that the DFT slightly differs from the theoretical continuous Fourier so that D_{mn} does not strictly equal $T_{\boldsymbol{k}_{mn}}$. In particular, the DFT deals with amplitudes for modes $\boldsymbol{k}_{mn}$ that are outside the Nyquist range and in some directions θ_{mn} only (see Fig. 1). It is therefore not possible to integrate Eq. (4) on the full range $[0, 2\pi]$ for such modes and so, the 1D-power spectrum is undefined outside the Nyquist range. In the following, we will therefore restrict to the Nyquist range for power spectrum estimation. Note however, that mathematical sums implied in the following may still run over the full ranges of pixels or DFT amplitude indices.

The direct DFT of the masked data result from the convolution of the DFT amplitudes by a kernel that depends only on the mask DFT amplitudes (see sect. 2.5 for a more detailed discussion) and whose determination is detailed in Appendix A. If the data D consist of signal T and noise N, we have

$$\langle|\hat{D}_{mn}|^2\rangle = \sum_{m'n'} |K^{n,n'}_{m,m'}|^2 |T_{m'n'}|^2 + \langle\hat{N}_{mn}\rangle. \tag{10}$$

Eq. (10) is the transcription in discrete space of Eq. (6).

The rapid oscillations of the convolution kernel introduce strong correlations between spatial frequencies and make its inversion numerically intractable. (*Pseudo-*)Power spectra are therefore estimated on some frequency band-powers (labelled b hereafter). The binning operator reads

$$R_b^{mn} = \begin{cases} \frac{k^\beta_{mn}}{\Xi_b} & \text{if } k^b_{low} \leq k_{mn} < k^{b+1}_{low} \\ 0 & \text{otherwise} \end{cases} . \tag{11}$$

k^b_{low} is the mode of lowest modulus that belongs to bin b and Ξ_b is the number of wave vectors $\boldsymbol{k}_{mn}$ that fall into the bin b. The reciprocal operator that relates the theoretical value of the one-dimensional binned power spectrum P_b to its value at $\boldsymbol{k}_{mn}$ is

$$Q^b_{mn} = \begin{cases} \frac{1}{k^\beta_{mn}} & \text{if } k^b_{low} \leq k_{mn} < k^{b+1}_{low} \\ 0 & \text{otherwise} \end{cases} . \tag{12}$$

Although not strictly required, results may be improved when the spectral index β is chosen so that $k^\beta P_k$ is as flat as possible[1]. In the case of Cosmic Infrared Background anisotropy, $\beta \simeq 1$ (Planck Collab. 2011). The binned *pseudo*-power spectra therefore reads

[1] In the case of CMB, $\beta \simeq 2$ is the equivalent of the standard $\ell(\ell+1)$ prefactor that flattens the spectrum up to $\ell \sim 2000$.

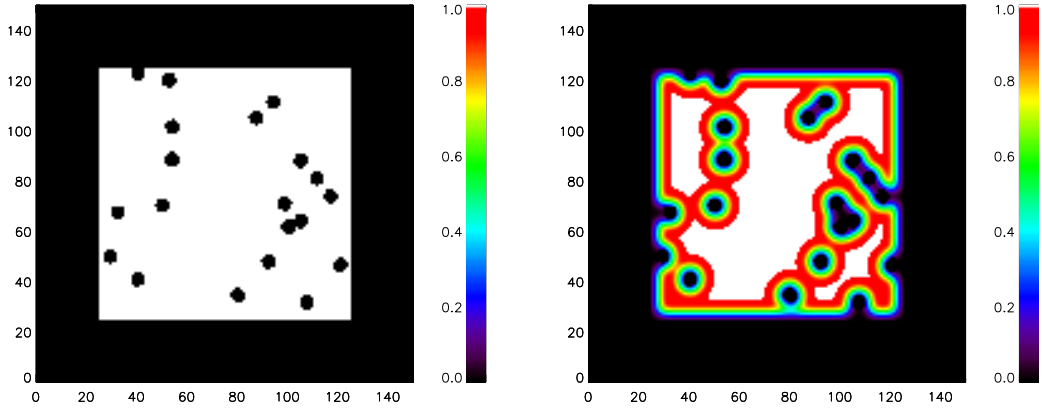

Figure 2. *Top:* Mask applied to the simulated data. This mask is 1 where data are available, 0 outside the observation patch and where bright sources have been masked out. *Bottom:* Same mask but with apodized boundaries. The apodization is done with a Gaussian kernel in a way that only affects "observed" pixels: the fraction of the mask that is strictly zero is not artificially reduced.

$$\hat{P}_b = \sum_{m,n\in b} R_b^{mn} |\hat{T}_{mn}|^2, \tag{13}$$

and the data power spectrum is related to its binned value P_b via

$$|T_{m'n'}|^2 \simeq Q^{b'}_{m'n'} P_{b'}. \tag{14}$$

With such binned quantities, Eq. (10) reads

$$\langle \hat{P}_b \rangle \simeq \sum_{b'} M_{bb'} P_{b'} + \langle \hat{N}_b \rangle, \tag{15}$$

with

$$M_{bb'} = \sum_{m,n\in b} \sum_{m',n'\in b'} R_b^{mn} |K^{n,n'}_{m,m'}|^2 Q^{b'}_{m'n'}. \tag{16}$$

An unbiased estimate of the binned angular power spectrum of the signal is thus given by

$$\tilde{P}_b \simeq \sum_{b'} M^{-1}_{bb'} \left(\hat{P}_{b'} - \langle \hat{N}_{b'} \rangle \right). \tag{17}$$

It is indeed easily checked that $\langle \tilde{P}_b \rangle = P_b$. Uncertainties on $\tilde{P}_b$ come from sampling and noise variance that are estimated via Monte-Carlo simulations as described in the next section.

2.4. Statistical uncertainties

Statistical uncertainties on P_b come from signal sampling variance and noise variance. They are described by stochastic processes of known power spectra and are obtained via Monte-Carlo simulations. For each realization, a map of signal+noise is produced and treated in the same way as described for the data in the previous section to give an estimate $\tilde{P}_b$ with the same statistical properties as that of the true data. Altogether, these simulations provide the uncertainties on our estimate. Indeed, the covariance matrix of $\tilde{P}_b$ is

$$\mathbf{C}_{bb'} = \left\langle \left(\tilde{P}_b - \langle \tilde{P}_b \rangle_{\rm MC} \right) \left(\tilde{P}_{b'} - \langle \tilde{P}_{b'} \rangle_{\rm MC} \right) \right\rangle_{\rm MC}, \tag{18}$$

with $\langle \cdot \rangle_{\rm MC}$ standing for Monte-Carlo averaging. The error bar on each $\tilde{P}_b$ is

$$\sigma_{\tilde{P}_b} = \sqrt{\mathbf{C}_{bb}}, \tag{19}$$

and the bin-bin correlation matrix is given by its standard definition

$$\mathbf{\Xi}_{bb'} = \frac{\mathbf{C}_{bb'}}{\sqrt{\mathbf{C}_{bb}\mathbf{C}_{b'b'}}}. \tag{20}$$

2.5. Beam, Map Making and Transfer Functions

The above sections describe the main features of the algorithm that provides an unbiased estimate of the power spectrum of data projected on a map. This power spectrum may however differ from the *signal* power spectrum. Indeed, the map making process may alter the statistical properties of the signal, together with filtering and the convolution by the instrumental beam. In the case of CMB anisotropy for which power spectrum estimation has been most extensively studied, to a good approximation, the transfer function F_k of the map making and the filtering together reduces to a function of k that multiplies the data power spectrum P_k. For instance, a minimal effect of the map making is due to pixelization that is equivalent to a convolution in real space by a square kernel and therefore translates into a multiplication in Fourier space. The effect of filtering can be determined by a set of Monte-Carlo simulations of timeline processing and map making. The beam smearing effect is also described by a multiplicative function B_k. In the present framework it is possible to be even more precise and to account for the exact beam shape and orientation since the beam can be completely described by its Fourier coefficients B_{mn} rather than by its approximated annular average B_k. This may be of particular relevance for small fields over which the scanning strategy of the instrument is approximately constant and increases the effect of beam asymmetry. The map making together with the filtering transfer function is also likely to be more accurately represented by a function of both Fourier indices F_{mn}, so that Eq. (10) actually reads

$$\begin{aligned}\langle|\hat{D}_{mn}|^2\rangle = & \sum_{m'n'} |K^{n,n'}_{m,m'}|^2 F_{m'n'} B_{m'n'} P_{\boldsymbol{k}_{m'n'}} \\ & + \langle\hat{N}(\boldsymbol{\ell}_{mn})\rangle, \end{aligned} \tag{21}$$

These new contributions can be absorbed in the definition of the convolution kernel $K^{n,n'}_{m,m'}$ so that no further modification of the algorithm is needed from Eq. (10) onward.

2.6. Algorithm

A scheme of the algorithm is proposed on Fig. 6. To run the complete process of power spectrum and statistical uncertainties estimation, one needs:

(a) A tool to generate maps of a given power spectrum
(b) A tool to compute the power spectrum of a 2D map and to bin it into a set of predefined bins with a weight that may be a function of k.
(c) A tool to compute $M_{bb'}$. It involves the computation of the convolution kernel $K^{n,n'}_{m,m'}$. This is actually the longest part of the work since it is a N^2_{pix} operation, but it only needs to be done once.

All these tools are provided in the POKER library[2]. The algorithm can be summarized as follows:

1. Insert the observed sky patch of size $N_x \times N_y$ pixels into a "large patch" ($N'_x \times N'_y$) and padd it with zeros. This will allow for the correction of aliasing by scales larger than the observed sky. The size of the patch and the zero padding that should be used remains to be determined by the user. A factor 1.2 to 2 is enough for most cases. A compromise must be chosen between the uncertainty due to large scales that the user tries to estimate and the uncertainty associated to the unknown power in these larges scales that needs to be assumed for the simulations. It is also possible to apodize the observation patch to limit large scale aliasing (see Sect. 3 for more details). When there are no holes in the observed patch and when noise is subdominant, this can improve the bin to bin correlation at high k.
2. Define a binning for the estimated power spectrum on the large patch. Typically, modes sampled by the data set are the DC level and modes between $k_{min} = 2\pi/\Delta\theta/\max(N_x, N_y)$ and the Nyquist mode $k_c = \pi/\Delta\theta$. The minimum bandwidth of the bins may be chosen as $\sim 2k_{min}$.
3. Determine the noise *pseudo*-power spectrum – $\langle\hat{N}_b\rangle$ of Eq. (15). If it cannot be determined analytically, run a set of Monte-Carlo realization of noise only maps (with (a)) and compute the power spectrum with (b) of the masked maps inserted into the large patch. The average of these Monte-Carlo realizations gives $\langle\hat{N}_b\rangle$.
4. Compute $M_{bb'}$ with (c) – Eqs (11, 12, 16). This operation scales like N^2_p but it only needs to be done once. The implementation proposed in the POKER library can be run on a multiprocessor machine.
5. Compute the *pseudo*-power spectrum of the masked data on the large patch $\hat{P}_b$ with (b) – Eq. (A.1).
6. Apply Eq. (17) to obtain the binned power spectrum of the data P_b. The resolution of this equation can be done with any suitable tool of linear algebra. Note that $M_{bb'}$ can be rather small and its inversion straightforward with standard numerical tools and to compute Eq. 17 as is. At this stage, it may be useful to discard the first bin of the matrix. Indeed, it describes the coupling of the DC level in the map and is therefore irrelevant for a power spectrum analysis whereas it tends to alter the conditioning of $M_{bb'}$.

[2] `http://www.ias.u-psud.fr/poker`. This library makes use of some of the HEALPix programs (Gorski et al 1998).

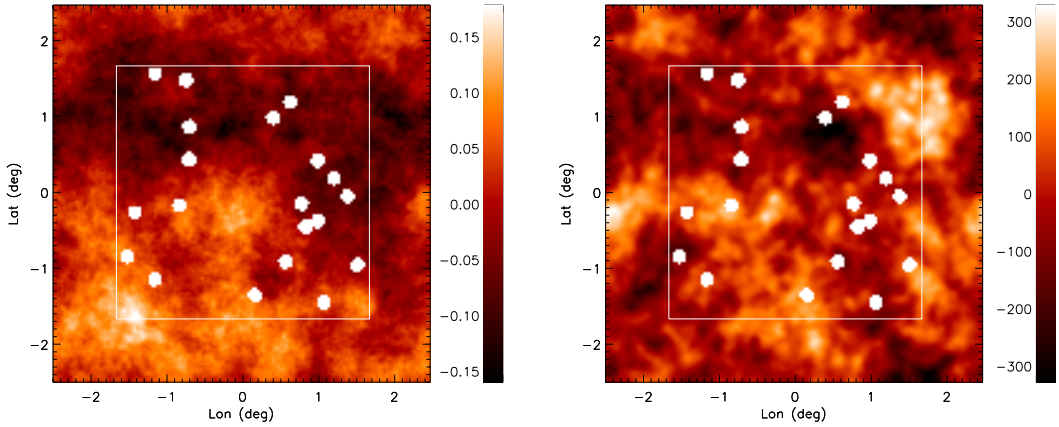

Figure 3. Typical maps of dust with a k^{-3} power spectrum (top) and CMB temperature (bottom). The square is the outline of the observed patch. It is extracted from a larger simulated map to ensure non periodic boundary conditions. Masked data appear in white.

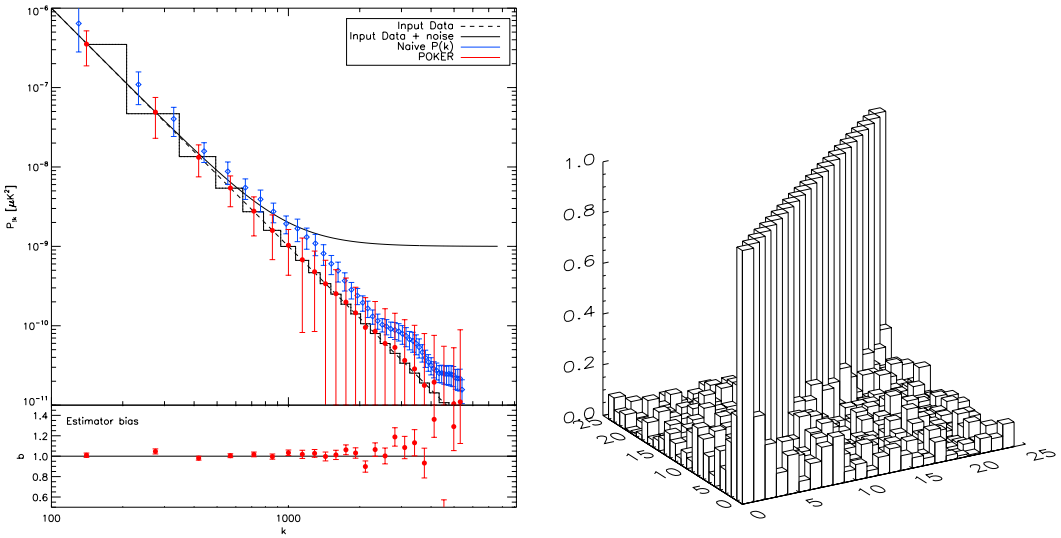

Figure 4. Dust (k^{-3}). Comparison between the input theoretical power spectrum (black) and the average result of POKER (red) applied to 500 signal+noise simulations. The "naive" approach (blue, see text) is also shown for reference. Error bars on the top plots are those associated to the data (i.e. those of a single realization). The square line shows the binned theoretical power spectrum to which POKER's average result should be compared. The bottom plots shows the ratio of the reconstructed binned power spectrum to the input theoretical binned power spectrum (the bias) and the displayed error bar is that of the average of the Monte-Carlo realization (in other words: the error bar of the top plot divided by $\sqrt{500}$). These plots altogether show that POKER is unbiased. The mask used in this case is that of the top plot of Fig. 2, with 1 where data are available, 0 elsewhere.

7. Determine the statistical error bars associated to this estimate. For that, run a set of Monte-Carlo realizations of signal+ noise. The input spectrum required for these simulations can be a smooth interpolation of the binned power spectrum determined at the previous step. For each realization, compute the *pseudo*-power spectrum (using (b) on the masked data embedded in the large patch), subtract $\langle \hat{N}_b \rangle$, solve Eq. (17). This provides a set of random realizations of $\tilde{P}_b$. The error bars and the bin to bin covariance matrix are then given by Eqs. (18,19).

3. Worked example

POKER was applied to real data to measure the Cosmic Infrared Background anisotropy in the Planck-HFI data (Planck Collab. 2011). In complement, we here present more limited worked examples on simulated data but with steeper power spectra and a more complex mask. Indeed, it is in this context that mask aliasing effects are the strongest.

We assume that the observation patch is a square of 100 pixels of 2 arcmin side. These parameters are chosen so that they sample a range of angular modes over which the CMB temperature power spectrum exhibits peaks and a

varying slope. Note however that the map resolution can be arbitrary high since Fast Fourier Transform algorithms work in dimensionless units. To force non periodic boundary conditions, we extract the patch from a map that is 50% larger and the simulation is performed on the latter. At last, we draw random holes across the observation patch to mimic point source masking. We consider two types of signal. In the first case, we assume that the data are represented by a pure power law spectrum k^{-3} typical of Galactic dust emission. In the second case, we assume that the data are CMB with a standard ΛCDM power spectrum. At these angular scales, the slope of the CMB power spectrum varies from $\sim k^{-2}$ to even steeper than k^{-6} and exhibits oscillations. Fig. 3 shows an example of such simulated data. The result of POKER applied to each case is presented on Figs. 4 and 5. In the case of dust, we choose a binning index $\beta = 3$ as defined in Eq. (12), in the case of CMB, we do not make any assumption, *i.e.* we choose $\beta = 0$. We also show what the direct Fourier transform of the observed patch without further correction would give to illustrate the magnitude of the effect corrected by POKER. Note that this reference estimate labelled "Naive $P(k)$" is not the *pseudo*-power spectrum of the data in the sense of Sect. 2. Indeed, it is not computed on the whole map from which the observation patch is extracted and padded with zeros. The bottom plots of Figs. 4 and 5 show the bin to bin correlation matrix of each estimate. In the case of dust, the correlations are small ($\sim 15\%$). This is not the case for the simulated CMB, for which there is strong bin to bin correlation, although the power spectrum remains unbiased. This correlation is due to large scale aliasing induced by the holes in the mask and show up so significantly because at high k, the CMB spectrum is very steep. A way to improve on this is to apodize the mask around the edges and the holes left by point source masking (Fig. 2). In this work, we simply use a Gaussian kernel with a FWHM of twice the map resolution to smooth the edges. The same analysis as before is performed with this mask and results are presented on the right hand of Fig. 5. This time, the bin to bin correlation is significantly reduced, albeit a slight increase in sampling variance at low k due to the effective reduction of the observation area. A more performant way to do such apodization is described in Grain et al 2009. Finally, on larger angular scales, there is a slight bias in the recovery of the CMB power spectrum that does not show up in the case of dust. It is because in the particular case of pure power law spectrum, Eq. (14) is an equality. It is no longer the case for a CMB spectrum whose average slope varies with k and exhibits peaks. No binning could faithfully represent such a spectrum. However, the remaining bias is negligible compared to the statistical error bar of the data. If we force the simulated CMB to have a constant power spectrum over frequency bins, the recovery is unbiased. There is no general prescription regarding the definition of the binning and the apodization. They must however be chosen with care since the bin to bin residual correlation may lead to residual ringing (mask aliasing) on the data power spectrum (considered as a single random realization), even if the estimator is unbiased on average.

4. Conclusion

We have developed a tool that provides an unbiased estimate of the angular power spectrum of diffuse emission in the flat sky approximation limit, for arbitrary high resolution and complex masks. POKER corrects for mask aliasing effects, even in the context of steep power spectra and provides a way to estimate statistical error bars and bin to bin correlations. It complements tools developed in the context of spherical sky and potentially full sky surveys (e.g. Hivon et al 2002) but for lower angular resolutions at the moment. POKER is also complementary to other methods in the flat sky approximation such as Das et al 2009.

POKER can readily be generalized to polarization power spectra estimation. To date, experiments that have measured polarized diffuse emission (Kovac et al 2002, Kogut et al 2003, Ponthieu et al 2005, Ade et al 2008, Chiang et al 2010, Bierman et al 2011) were closely related to CMB experiments, they had observation patches of few to hundred percents of the sky and angular resolutions larger than a few arcmin. Optimal tools have been developed to measure the polarization power spectra in this context (Chon et al 2004, Smith 2006, Smith & Zaldarriaga 2007, Grain et al 2009 and references therein) and it is unlikely that POKER would bring something significantly new for such observations. It is however expected that smaller, deeper and higher resolution polarized surveys will happen in the future, for which POKER might be an interesting approach. One of the main features that should then be addressed is the ability of POKER to correct for $E - B$ leakage. Although we postpone the detailed studies of POKER's properties regarding polarized power spectra estimation for a future work, we provide the formalism in Appendices B and C for the sake of completeness. All the software used in this work is publicly available at `http://www.ias.u-psud.fr/poker`.

Acknowledgements. We thank E. Hivon, O. Doré, S. Prunet, K. Benabed, C. Rosset and T. Rodet for fruitful discussions. J. Grain was supported by the "Groupement d'Intérêt Scientifique (GIS) Physique des 2 Infinis (P2I). This research used resources of the National Energy Research Scientific Computing Center, which is supported by the Office of Science of the U.S. Department of Energy under Contract No. DE-AC02-05CH11231.

References

Ade, P., Bock, J., Bowden, M., et al, 2008, ApJ, 674, 22
Bond, J. R., Jaffe, A. H., Knox, L., Phys Rev D, 57, 2117-2137
Benît, A., Ade, P., Amblard, A. et al, 2003, AA, 399, L25
Bierman, E. M., et al, 2011, ApJ, submitted, `astro-ph/1103.0289`
Brown, M., Ade, P., Bock, J., et al, 2009, ApJ, 705, 978
Chiang, H. C., Ade, P., Barkats, D. et al, 2010, ApJ 711, 1123-1140
Chon, G., Challinor, A., Prunet, S., Hivon, E., 2004, MNRAS, 350, 914
Das, S., Hajian, A., Spergel, D. N., 2009, Phys. Rev. D 79, 083008
de Bernardis, P., et al, 2000, Nature, 404, 955

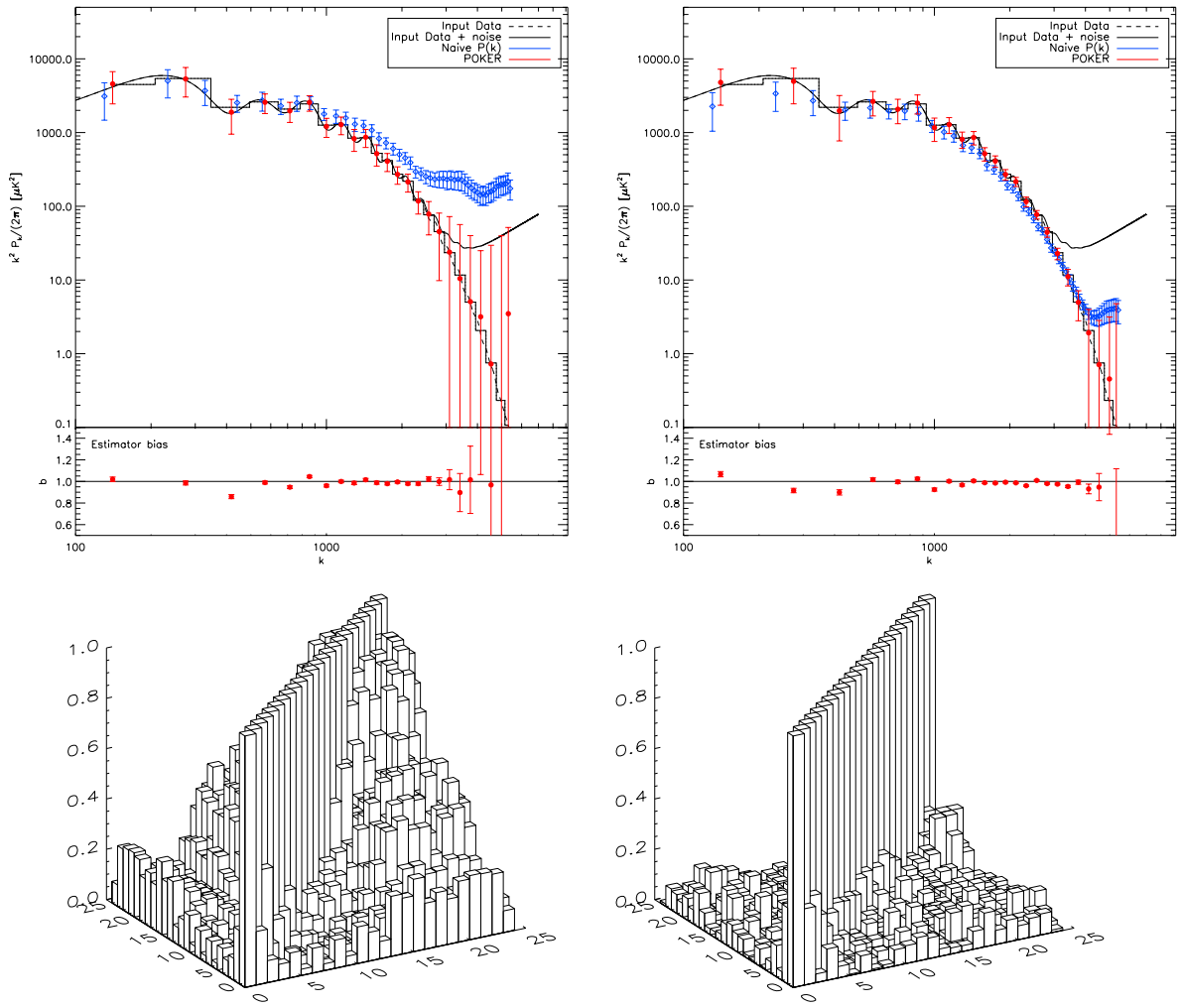

Figure 5. *Left*: same as Fig. 4 in the case of CMB. POKER's estimation is unbiased but mask aliasing induces strong correlations between bins at high k where the power spectrum is very steep. *Right*: This time, the mask with apodized boundaries (bottom of Fig. 2) is used. High k bin to bin correlations are significantly reduced. Apodization however reduces the effective observed fraction of the sky and therefore slightly increases error bars at low k compared to the plots on top. Note that although apodization also improves the "naive" estimate, it remains not compatible with the input spectrum for almost every bin and to more than the 1σ error of a single realization.

Grain, J., Tristram, M., Stompor, R., Phys Rev D79, 123515
Gorski, K., M., Hivon, E., Wandelt, B., D., 1998, in Evolution of Large Scale Structure, ed A. J. Banday, R. K. Sheth & L. Da Costa Garching:ESO, 37
Hikage, C., Takada, M., Hamana, T., Spergel, D. N., `astro-ph/1004.3542`
E. Hivon, K.M. Górski, C.B. Netterfield, B.P. Crill, S. Prunet, & F. Hansen, 2002, Astrophys. J., **567**, 2
Hinshaw, G., Spergel, D., Verde, L. et al, 2003, ApJS, 148, 135
Kogut, A., Spergel, D., Barnes, C., et al, 2003, ApJS, 148, 161
Kovac, J., Leitch, E., Pryke, C., et al, 2002, Nature, 420, 772-787
Miville-Deschênes, M.-A., Lagache, G., Boulanger, F., Puget, J.-L., 2007, AA, 469, 595
`http://www.nr.com`
Planck Collaboration, 2011, Planck early results 18: The Power Spectrum of the Cosmic Infrared Background, AA submitted, `astro-ph/1101.2028`
Ponthieu, N., Macìas-Pérez, J.-F., Tristram, M., et al, 2005, AA, 444, 327
Pryke, C., Ade., P., Bock. J., et al, 2009, ApJ, 692, 1247-1270
Reichardt, C., Ade, P., Bock., J. et al, 2009, ApJ, 694, 1200
Smith, K. M., 2006, Phys. Rev. D, 74, 083002
Smith, K. M., Zaldarriaga, M., 2007, Phys. Rev. D, 76, 043001
Tristram, M., Patanchon, G., Macìas-Pérez, J.-F., et al, 2005, AA, 436, 785

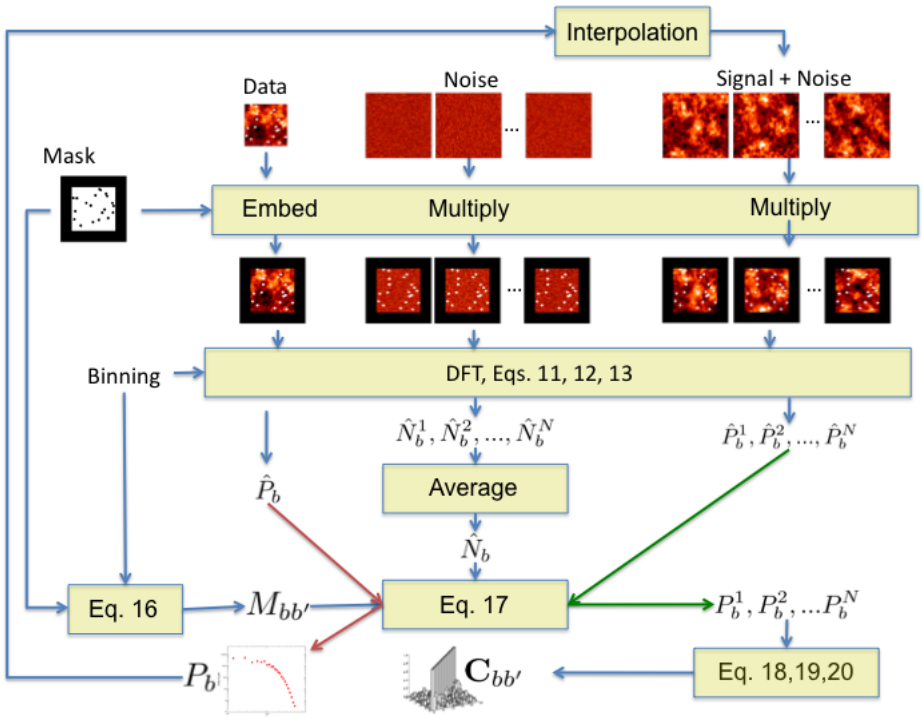

Figure 6. Schematic flow chart of POKER.

Appendix A: Mask convolution kernel for Temperature

If not specified, sums run from 0 to $N_x - 1$ and 0 to $N_y - 1$. The *pseudo*-Fourier coefficients of the weighted data read

$$\begin{aligned}\hat{T}_{mn} &= \frac{1}{N_x N_y}\sum_{\mu,\nu} T_{\mu\nu} W_{\mu\nu} e^{-2i\pi(\mu m/N_x + \nu n/N_y)}, \qquad \text{(A.1)}\\ &= \frac{1}{N_x N_y}\sum_{\mu,\nu}\sum_{m_1,n_1} T_{m_1 n_1} e^{2i\pi(\mu m_1/N_x+\nu n_1/N_y)} \sum_{m_2,n_2} W_{m_2 n_2} e^{2i\pi(\mu m_2/N_x+\nu n_2/N_y)} e^{-2i\pi(\mu m/N_x+\nu n/N_y)},\\ &= \frac{1}{N_x N_y}\sum_{m_1,n_1,m_2,n_2}\sum_{\mu,\nu} T_{m_1 n_1} W_{m_2 n_2} e^{2i\pi[\mu(m_1 N_x + m_2 - m)/N_x + \nu(n_1+n_2-n)/N_y]}. \qquad \text{(A.2)}\end{aligned}$$

$m_1 + m_2$ belongs to $[0, 2N_x - 2]$, so

$$\sum_{\mu=0}^{N_x-1} e^{2i\pi\mu(m_1+m_2-m)/N_x} = N_x \delta_{m_2}^{m-m_1} + N_x \delta_{m_2}^{N_x+m-m_1}. \qquad \text{(A.3)}$$

Similar relations hold for indices n, hence

$$\hat{T}_{mn} = \sum_{m_1,n_1,m_2,n_2} T_{m_1 n_1} W_{m_2 n_2} \left(\delta_{m_2}^{m-m_1} + \delta_{m_2}^{N_x+m-m_1}\right)\left(\delta_{n_2}^{n-n_1} + \delta_{n_2}^{N_y+n-n_1}\right). \qquad \text{(A.4)}$$

Equation (8) specifies that Fourier coefficients are only defined for $m, n \in [0, N_x] \times [0, N_y]$, hence

$$\hat{T}_{mn} = \sum_{m_1,n_1} T_{m_1,n_1} K_{m,m_1}^{n,n_1} \qquad \text{(A.5)}$$

with

$$K_{m,m_1}^{n,n_1} = \begin{cases} W_{m-m_1,\,n-n_1} & \text{if } m_1 \le m \text{ and } n_1 \le n \\ W_{m-m_1,\,N_y+n-n_1} & \text{if } m_1 \le m \text{ and } n_1 > n \\ W_{Nx+m-m_1,\,n-n_1} & \text{if } m_1 > m \text{ and } n_1 \le n \\ W_{Nx+m-m_1,\,N_y+n-n_1} & \text{if } m_1 > m \text{ and } n_1 > n \end{cases}. \qquad \text{(A.6)}$$

Appendix B: Mask convolution kernel for Polarization only

Polarization maps are represented in direct space by Stokes parameters Q and U, in angular space by E and B. These parameters are related by

$$Q_{\mu\nu} = \sum_{m_1,n_1} \left[\cos(2\phi^{\mu\nu}_{m_1n_1})E_{m_1n_1} - \sin(2\phi^{\mu\nu}_{m_1n_1})B_{m_1n_1}\right] e^{2i\pi(\mu m_1/N_x+\nu n_1/N_y)} \quad (B.1)$$

$$U_{\mu\nu} = \sum_{m_1,n_1} \left[\sin(2\phi^{\mu\nu}_{m_1n_1})E_{m_1n_1} + \cos(2\phi^{\mu\nu}_{m_1n_1})B_{m_1n_1}\right] e^{2i\pi(\mu m_1/N_x+\nu n_1/N_y)}, \quad (B.2)$$

The polarization *pseudo*-Fourier coefficients read

$$\hat{E}_{mn} = \frac{1}{N_xN_y}\sum_{\mu,\nu}\left[\cos(2\phi^{\mu\nu}_{mn})Q_{\mu\nu} + \sin(2\phi^{\mu\nu}_{mn})U_{\mu\nu}\right] W_{\mu\nu}e^{-2i\pi(\mu m/N_x+\nu n/N_y)}, \quad (B.3)$$

$$= \frac{1}{N_xN_y}\sum_{m_1,n_1}\sum_{m_2,n_2}\sum_{\mu,\nu} W^{n_2}_{m_2}\left[\cos\left(2\phi^{\mu\nu}_{mn} - 2\phi^{\mu\nu}_{m_1n_1}\right)E_{m_1n_1} + \sin\left(2\phi^{\mu\nu}_{mn} - 2\phi^{\mu\nu}_{m_1n_1}\right)B_{m_1n_1}\right] \quad (B.4)$$
$$\times e^{2i\pi(\mu m_1/N_x+\nu n_1/N_y)}e^{2i\pi(\mu m_2/N_x+\nu n_2/N_y)}e^{-2i\pi(\mu m/N_x+\nu n/N_y)},$$

$$\hat{B}_{mn} = \frac{1}{N_xN_y}\sum_{\mu,\nu}\left[-\sin(2\phi^{\mu\nu}_{mn})Q_{\mu\nu} + \cos(2\phi^{\mu\nu}_{mn})U_{\mu\nu}\right] W_{\mu\nu}e^{-2i\pi(\mu m/N_x+\nu n/N_y)}, \quad (B.5)$$

$$= \frac{1}{N_xN_y}\sum_{m_1,n_1}\sum_{m_2,n_2}\sum_{\mu,\nu} W^{n_2}_{m_2}\left[-\sin\left(2\phi^{\mu\nu}_{mn} - 2\phi^{\mu\nu}_{m_1n_1}\right)E_{m_1n_1} + \cos\left(2\phi^{\mu\nu}_{mn} - 2\phi^{\mu\nu}_{m_1n_1}\right)B_{m_1n_1}\right] \quad (B.6)$$
$$\times e^{2i\pi(\mu m_1/N_x+\nu n_1/N_y)}e^{2i\pi(\mu m_2/N_x+\nu n_2/N_y)}e^{-2i\pi(\mu m/N_x+\nu n/N_y)}.$$

We now have to compute the following two summations

$$I_1 = \sum_{\mu,\nu}\cos\left(2\phi^{\mu\nu}_{mn} - 2\phi^{\mu\nu}_{m_1n_1}\right)e^{2i\pi(\mu m_1/N_x+\nu n_1/N_y)}e^{2i\pi(\mu m_2/N_x+\nu n_2/N_y)}e^{-2i\pi(\mu m/N_x+\nu n/N_y)}, \quad (B.7)$$

$$I_2 = \sum_{\mu,\nu}\sin\left(2\phi^{\mu\nu}_{mn} - 2\phi^{\mu\nu}_{m_1n_1}\right)e^{2i\pi(\mu m_1/N_x+\nu n_1/N_y)}e^{2i\pi(\mu m_2/N_x+\nu n_2/N_y)}e^{-2i\pi(\mu m/N_x+\nu n/N_y)}. \quad (B.8)$$

Because $\phi^{\mu\nu}_{mn}$ is the angle between $\boldsymbol{k}_{mn}$ and $\boldsymbol{r}_{\mu\nu}$ and $\phi^{\mu\nu}_{m_1n_1}$ is the angle between $\boldsymbol{k}_{m_1n_1}$ and $\boldsymbol{r}_{\mu\nu}$, we have $\phi^{\mu\nu}_{mn} - \phi^{\mu\nu}_{m_1n_1} = \phi^{mn}_{m_1n_1}$ with

$$\cos(\phi^{m_1n_1}_{mn}) = \boldsymbol{k}_{m_1n_1}\cdot\boldsymbol{k}_{mn}.$$

As a consequence, the sine and cosine do not depend on pixel indices, μ and ν, so we can use the orthogonality relation used for temperature, i.e. $\forall\ m_1+m_2$ belongs to $[0, 2N-2]$:

$$\sum_{\mu=0}^{N-1} e^{2i\pi\mu(m_1+m_2-m)/N_x} = N_x\delta^{m-m_1}_{m_2} + N_x\delta^{N+m-m_1}_{m_2},$$

to finally get

$$\hat{E}_{mn} = \sum_{m_1,n_1} K^{n,n_1}_{m,m_1}\left[\cos\left(2\phi^{m_1n_1}_{mn}\right)E_{m_1n_1} + \sin\left(2\phi^{m_1n_1}_{mn}\right)B_{m_1n_1}\right], \quad (B.9)$$

$$\hat{B}_{mn} = \sum_{m_1,n_1} K^{n,n_1}_{m,m_1}\left[-\sin\left(2\phi^{m_1n_1}_{mn}\right)E_{m_1n_1} + \cos\left(2\phi^{m_1n_1}_{mn}\right)B_{m_1n_1}\right]. \quad (B.10)$$

From this last results, we can compute the *pseudo*-power spectra, keeping in mind that

$$\left\langle E^n_m E^*_{m'n'}\right\rangle = C^{EE}_{mn}\delta_{m,m'}\delta_{n,n'},$$
$$\left\langle B^n_m B^*_{m'n'}\right\rangle = C^{BB}_{mn}\delta_{m,m'}\delta_{n,n'}$$

and

$$\left\langle E^n_m B^*_{m'n'}\right\rangle = \left\langle B^n_m E^*_{m'n'}\right\rangle = C^{EB}_{mn}\delta_{m,m'}\delta_{n,n'}.$$

We define the estimated *pseudo*-spectra as

$$\hat{P}^{EE}_{mn} = \left|\hat{E}_{mn}\right|^2,$$

$$C^{\hat{B}B}{}_{mn} = \left|\hat{B}_{mn}\right|^2$$

and

$$\hat{P}^{EB}_{mn} = \frac{1}{2}\left[\hat{E}_{mn}\hat{B}^*_{mn} + \hat{B}_{mn}\hat{E}^*_{mn}\right] = \mathrm{Re}\left[\hat{E}_{mn}\hat{B}^*_{mn}\right] = \mathrm{Re}\left[\hat{B}_{mn}\hat{E}^*_{mn}\right].$$

By using those definitions, we can easily show that

$$\hat{P}^{EE}_{mn} = \sum_{m_1,n_1}|K^{n,n_1}_{m,m_1}|^2\left[\cos^2\left(2\phi^{m_1n_1}_{mn}\right)C^{EE}_{m_1n_1} + \sin^2\left(2\phi^{m_1n_1}_{mn}\right)C^{BB}_{m_1n_1} + \sin\left(4\phi^{m_1n_1}_{mn}\right)C^{EB}_{m_1n_1}\right],$$

$$\hat{P}^{BB}_{mn} = \sum_{m_1,n_1}|K^{n,n_1}_{m,m_1}|^2\left[\sin^2\left(2\phi^{m_1n_1}_{mn}\right)C^{EE}_{m_1n_1} + \cos^2\left(2\phi^{m_1n_1}_{mn}\right)C^{BB}_{m_1n_1} - \sin\left(4\phi^{m_1n_1}_{mn}\right)C^{EB}_{m_1n_1}\right],$$

$$\hat{P}^{EB}_{mn} = \sum_{m_1,n_1}|K^{n,n_1}_{m,m_1}|^2\left[-\frac{1}{2}\sin\left(4\phi^{m_1n_1}_{mn}\right)C^{EE}_{m_1n_1} + \frac{1}{2}\sin\left(4\phi^{m_1n_1}_{mn}\right)C^{BB}_{m_1n_1} + \left(\cos^2\left(2\phi^{m_1n_1}_{mn}\right) - \sin^2\left(2\phi^{m_1n_1}_{mn}\right)\right)C^{EB}_{m_1n_1}\right].$$

In a matrix formulation, this reads

$$\begin{pmatrix} \hat{P}^{EE}_{mn} \\ \hat{P}^{BB}_{mn} \\ \hat{P}^{EB}_{mn} \end{pmatrix} = \sum_{m_1,n_1} \begin{pmatrix} M^{EE,EE}_{mn,m_1n_1} & M^{EE,BB}_{mn,m_1n_1} & M^{EE,EB}_{mn,m_1n_1} \\ M^{BB,EE}_{mn,m_1n_1} & M^{BB,BB}_{mn,m_1n_1} & M^{BB,EB}_{mn,m_1n_1} \\ M^{EB,EE}_{mn,m_1n_1} & M^{EB,BB}_{mn,m_1n_1} & M^{EB,EB}_{mn,m_1n_1} \end{pmatrix} \begin{pmatrix} P^{EE}_{m_1n_1} \\ P^{BB}_{m_1n_1} \\ P^{EB}_{m_1n_1} \end{pmatrix} \tag{B.11}$$

$$= \sum_{m_1,n_1} \begin{pmatrix} M^{diag}_{mn,m_1n_1} & M^{off}_{mn,m_1n_1} & M^{cross}_{mn,m_1n_1} \\ M^{off}_{mn,m_1n_1} & M^{off}_{mn,m_1n_1} & -M^{cross}_{mn,m_1n_1} \\ -\frac{1}{2}M^{cross}_{mn,m_1n_1} & \frac{1}{2}M^{cross}_{mn,m_1n_1} & M^{diag}_{mn,m_1n_1} - M^{off}_{mn,m_1n_1} \end{pmatrix} \begin{pmatrix} P^{EE}_{m_1n_1} \\ P^{BB}_{m_1n_1} \\ P^{EB}_{m_1n_1} \end{pmatrix}, \tag{B.12}$$

with

$$M^{diag}_{mn,m_1n_1} = \cos^2(2\phi^{m_1n_1}_{mn})|K^{n,n_1}_{m,m_1}|^2, \tag{B.13}$$

$$M^{off}_{mn,m_1n_1} = \sin^2(2\phi^{m_1n_1}_{mn})|K^{n,n_1}_{m,m_1}|^2, \tag{B.14}$$

$$M^{cross}_{mn,m_1n_1} = \sin(4\phi^{m_1n_1}_{mn})|K^{n,n_1}_{m,m_1}|^2. \tag{B.15}$$

When the above mixing matrices are averaged over the two azimuthal (or polar for flat sky) angles, it can be shown that $\int\int M^{cross}_{mn,m_1n_1} d\theta d\theta_1 = 0$. However, before such an averaging, it is not *a priori* zero.

Appendix C: Mask convolution kernel for temperature polarization cross-correlation

For the cross-correlation of the temperature with CMB maps, we remind first that

$$\langle T_{mn} E^*_{m'n'} \rangle = \langle E_{mn} T^*_{m'n'} \rangle = C^{TE}_{mn} \delta_{m,m'} \delta_{n,n'}$$

and

$$\langle T_{mn} B^*_{m'n'} \rangle = \langle B_{mn} T^*_{m'n'} \rangle = C^{TB}_{mn} \delta_{m,m'} \delta_{n,n'}.$$

The estimated cross-*pseudo*-spectrum are defined as

$$\hat{P}^{TE}_{mn} = \frac{1}{2}\left[\hat{T}_{mn}\hat{E}^*_{mn} + \hat{E}_{mn}\hat{T}^*_{mn}\right] = \mathrm{Re}\left[\hat{T}_{mn}\hat{E}^*_{mn}\right] = \mathrm{Re}\left[\hat{E}_{mn}\hat{T}^*_{mn}\right]$$

and

$$\hat{P}^{TB}_{mn} = \frac{1}{2}\left[\hat{T}_{mn}\hat{B}^*_{mn} + \hat{B}_{mn}\hat{T}^*_{mn}\right] = \mathrm{Re}\left[\hat{T}_{mn}\hat{B}^*_{mn}\right] = \mathrm{Re}\left[\hat{B}_{mn}\hat{T}^*_{mn}\right].$$

From this and from the above defined *pseudo*-Fourier coefficients, we show that

$$\begin{pmatrix} \hat{P}^{TE}_{mn} \\ \hat{P}^{TB}_{mn} \end{pmatrix} = \sum_{m_1,n_1} \begin{pmatrix} M^{gaid}_{mn,m_1n_1} & M^{ffo}_{mn,m_1n_1} \\ -M^{ffo}_{mn,m_1n_1} & M^{gaid}_{mn,m_1n_1} \end{pmatrix} \begin{pmatrix} P^{TE}_{m_1n_1} \\ P^{TB}_{m_1n_1} \end{pmatrix}, \tag{C.1}$$

with

$$M^{gaid}_{mn,m_1n_1} = \cos(2\phi^{m_1n_1}_{mn})|K^{n,n_1}_{m,m_1}|^2, \tag{C.2}$$

$$M^{ffo}_{mn,m_1n_1} = \sin(2\phi^{m_1n_1}_{mn})|K^{n,n_1}_{m,m_1}|^2. \tag{C.3}$$

As is the case for the *cross* blocks in the polarization case, the azimuthal average of M^{ffo}_{mn,m_1n_1} is vanishing, i.e. $\int\int M^{ffo}_{mn,m_1n_1} d\theta d\theta_1 = 0$. However, before such an averaging, it is not *a priori* zero.